Science Advances
AAAS

advances.sciencemag.org/cgi/content/full/6/44/eabc9123/DC1

Supplementary Materials for

Algal plankton turn to hunting to survive and recover from end-Cretaceous impact darkness

Samantha J. Gibbs*, Paul R. Bown, Ben A. Ward, Sarah A. Alvarez, Hojung Kim, Odysseas A. Archontikis, Boris Sauterey, Alex J. Poulton, Jamie Wilson, Andy Ridgwell

*Corresponding author. Email: samantha.gibbs@noc.soton.ac.uk

Published 30 October 2020, *Sci. Adv.* **6**, eabc9123 (2020)
DOI: 10.1126/sciadv.abc9123

The PDF file includes:

Other Supplementary Material for this manuscript includes the following:

(available at advances.sciencemag.org/cgi/content/full/6/44/eabc9123/DC1)

Data file S1

A Matrix Community Model

The evolutionary ecosystem model represents a fixed-volume homogenous culture containing an arbitrary number of potential plankton phenotypes. The model environment is broadly analogous to a well-mixed ocean surface layer. Subsurface waters containing a fixed concentration of the limiting nutrient (N) are entrained into the surface layer at a constant rate (κ), with surface waters containing nutrients and plankton populations mixed out at an equivalent rate. Nutrients within the surface layer are taken up by the plankton community.

$$\frac{dN}{dt} = \kappa(N_0 - N) - \sum_{j=1}^{J} \mu_j B_j \quad (1)$$

Here μ_j and B_j are the gross biomass specific growth rate and nitrogen biomass of population j.

Plankton growth model

For a single plankton population, B (mmol N m^{-3}), the net biomass-specific population growth rate is represented by a generic growth equation that includes the potential for both autotrophic and heterotrophic growth, alongside losses to predation and a mortality term that includes a baseline value (δ) and density-dependent term ($B\delta$).

$$\frac{1}{B}\frac{dB}{dt} = \mu + \lambda \cdot G^{+} - G^{-} - (1 + B)\delta \quad (2)$$

Here, μ is the biomass-specific light and nutrient-limited growth from autotrophic metabolism, λ is the grazing assimilation efficiency, and G^{+} and G^{-} are the biomass-specific gains from prey and losses to predators, respectively.

Phototrophic growth: Autotrophic plankton growth is represented by the Monod (*74*) model, such that

$$\mu = \frac{\mu_{max} \cdot \alpha \cdot N}{\mu_{max} + \alpha \cdot N} \cdot \gamma \quad (3)$$

Here μ_{max} is the maximum autotrophic growth rate (d^{-1}), N is the environmental concentration of dissolved nitrate (mmol N m-3), and α is the biomass-specific nitrate affinity (m3 (mmol N)$^{-1}$ d^{-1}). The dimensionless light-limitation factor, γ, is simply a prescribed scalar that is set to a constant value.

Heterotrophic growth: The biomass-specific rate of predation approximates a linear "Holling type I" function (*75*) of prey biomass (B_{prey}), modified by the 'availability' of the prey to the predator, ϕ, and the grazing attack rate g. The attack rate is down-regulated at low total prey concentrations, providing a 'refuge' for prey that serves to dampen population instabilities (*76*).

$$g' = g \cdot (1 - e^{\Lambda \cdot \phi \cdot B_{prey}}) \quad (4)$$

Gains from predation (modified by λ in equation 1) are thus described by

$$G^{+} = g' \cdot \phi \cdot B_{prey} \quad (5)$$

Losses to predators are given by

$$G^{-} = g'_{pred} \cdot \phi \cdot B_{pred} \quad (6)$$

Phenotypic traits in the plankton community

We consider a community of J potential phenotypes. These are distributed across a two-dimensional trait space. The first trait dimension is made up of J_s geometrically-spaced plankton size classes between 0.6 µm and 6 mm ESD (equivalent spherical diameter). The second trait dimension is made up of J_t linearly-spaced trophic classes, defined by a dimensionless 'trophic index' (τ). This specifies a position along a 'trophic spectrum' spanning phytoplankton (τ=1), a range of mixotrophs (0<τ<1) and zooplankton (τ=0). These two 'master traits' govern a wider range of other important traits within the model, including those related to population growth and predator-prey interactions.

Size-dependent physiology: The size-dependent parameters of the growth model are assigned according to empirically- constrained allometric scaling laws (*64*, *77*), as defined in table S4a. While biomass-specific nitrate affinity and grazing clearance rates are reasonably well-described as power-law functions of cell volume (fig. S7), μ_{max} has been shown to follow a more complex monomodal relationship with cell volume (*77*, *78*). Here we approximate μ_{max} as a size-dependent function, governed by three empirically-constrained physiological parameters: the theoretical growth rate at infinite quota (μ^{∞}), the maximum cellular N uptake rate (ρ_{max}) and the minimum cellular N quota (Q_{min}). While these parameters are not resolved by the Monod model given in equation 2, they fully constrain μ_{max} under an assumption of cellular equilibrium (*79*, *80*), such that

$$\mu_{max} = \frac{\mu^{\infty} \cdot \rho_{max}}{\mu^{\infty} \cdot Q_{min} + \rho_{max}} \quad (7)$$

With μ^{∞}, ρ_{max} and Q_{min} constrained by observations (*77*, *80*), equation 7 yields a reasonable fit to measurements of μ_{max} (fig. S7a), with a monomodal size-dependence peaking at ~6 µm (*80*). Figure S7b and c are the assumed size-dependences of the biomass-specific nitrate affinity, α (*64*), and the grazing clearance rate, g (*62*).

Size-dependent interactions: Organism size also determines the availability of prey to predators, ϕ. This is an approximately log-normal function of the predator-prey volume ratio (θ), such that $\phi = 1$ when $\vartheta = \vartheta_{opt}$ (*81*), as shown in figure S7d.

$$\phi = \exp\left(-\left[\ln\left(\frac{\vartheta}{\vartheta_{opt}}\right)\right]^2 \cdot \frac{1}{2\phi_\sigma^2}\right) \quad (8)$$

Trade-off between autotrophy and heterotrophy: Organisms are positioned along a trophic spectrum between autotrophy and heterotrophy according to a trophic index, τ. Strictly autotrophic phytoplankton are assigned τ = 1, while strictly heterotrophic zooplankton are assigned τ = 0. If μ_{max} and g are the size-dependent maximum growth rates and grazing clearance rates of these phytoplankton and zooplankton specialists, the corresponding rates for all populations are given by

$$\mu_{max}(\tau) = \tau \cdot \mu_{max} \quad (9)$$

$$\mathrm{g}(\tau) = \tau \cdot g \quad (10)$$

Size-independent parameters are defined in table S4b.

Matrix notation

For mathematical and computational convenience, each phenotype in the two-dimensional trait space is assigned a single phenotypic index, $j = \{1,2,\ldots,J\}$, where $J = J_s \cdot J_t$. This indexing scheme allows all populations in the local community to be represented as a column vector,

$$\vec{B} = \begin{bmatrix} B_1 \\ B_2 \\ \vdots \\ B_J \end{bmatrix}$$

In a similar fashion, traits that vary among the community can also be written as vectors. For example, the nitrate affinities of every population in the community can now be written as

$$\vec{\alpha} = \begin{bmatrix} \alpha_1 \\ \alpha_2 \\ \vdots \\ \alpha_J \end{bmatrix}$$

Note that parameters remain as scalars if they are assumed to be equal for all phenotypes. Throughout the text, every vector is written underneath an arrow (e.g. $\vec{x}$) and every matrix is written in bold text (e.g. $\boldsymbol{x}$). Element-wise multiplication will always be denoted with a '$\cdot$' symbol. If no symbol is used between vectors or matrices, then the matrix product is used.

Ecological dynamics

Using the above notation, equation 2 can now be rewritten for the entire community as follows

$$\frac{1}{\vec{B}}\frac{d\vec{B}}{dt} = \vec{\mu} + \lambda \cdot \vec{G}^+ - \vec{G}^- - (1 + B)\delta \quad (11)$$

The gross autotrophic growth rate of the community is given by

$$\vec{\mu} = \frac{\vec{\mu}_{max} \cdot \vec{\alpha} \cdot P}{\vec{\mu}_{max} + \vec{\alpha} \cdot P} \cdot \gamma \quad (12)$$

and the community grazing terms are

$$\vec{G}^{+} = \vec{g}' \cdot \left(\boldsymbol{\phi}^{\mathrm{T}} \vec{B}\right) \quad (13)$$

$$\vec{G}^{-} = \boldsymbol{\phi}\left(\vec{B} \cdot \vec{g}'\right) \quad (14)$$

Here $\boldsymbol{\phi}$ is the $[J_{prey} \times J_{pred}]$ 'grazing kernel' describing the availability of each population (as prey) to each population (as a predator), as shown in figure S7d. In equation 13, $\boldsymbol{\phi}^{\mathrm{T}}\vec{B}$ describes the sum of all prey biomass available to each predator (where $\boldsymbol{\phi}^{\mathrm{T}}$ is the transpose of the grazing kernel). When multiplied by $\vec{g}'$, this gives the pre-assimilation grazing by each population on all available prey. The matrix product $\boldsymbol{\phi}\left(\vec{B} \cdot \vec{g}'\right)$ in equation 14 describes the total rate of predatory losses suffered by each prey. The grazing refuge is calculated according to the prey available to each predator, such that

$$\vec{g}' = \vec{g} \cdot (1 - e^{\Lambda \cdot [\boldsymbol{\phi}^{\boldsymbol{T}} \vec{B}]}) \quad (15)$$

Evolutionary dynamics

Adaptive evolution is enabled by allowing a small fraction of each population's net growth rate to be diverted to neighbouring phenotypes in the trait space (*67, 82*). In practice, this is achieved by adding a small mutational flux, $\vec{L}_e$ to equation 11, such that

$$\frac{d\vec{B}}{dt} = \left(\vec{\mu} + \lambda \cdot \vec{G}^{+} - \vec{G}^{-} - (1 + B)\delta\right) \cdot \vec{B} + \vec{L}_e \quad (16)$$

Each element in $\vec{L}_e$ describes the net flux of mutants in and out of each phenotypic class. We assume that mutants are produced as a fixed proportion of each population's gross growth rate, $\vec{\mu}_{ggr}$, where

$$\vec{\mu}_{ggr} = \left(\vec{\mu} + \lambda \cdot \vec{G}^{+}\right) \cdot \vec{B} \quad (17)$$

The mutational flux is calculated as the matrix product of $\vec{\mu}_{ggr}$ and the $[J \times J]$ mutation matrix, $\boldsymbol{E}$.

$$\vec{L}_e = \vec{\mu}_{ggr}\boldsymbol{E} \quad (18)$$

The mutation matrix itself is defined by the fraction of daughter cells in each population that, as mutants, are diverted to the neighbouring phenotypic class. This fraction could be a single value for both trait dimensions, but here we assume that the fractions σ_s and σ_t are diverted to adjoining phenotypes in the trophic and size dimensions, respectively. For a 51×51 trait space (J = 2061) the mutation matrix is extremely sparse, with a density of just under 0.2%. The mutation rate needs to be adjusted to account for the resolution of phenotypes (*67, 82*)

$$\sigma_s = \sigma \cdot (J_s - 1)^2 \tag{19}$$

$$\sigma_t = \sigma \cdot (J_t - 1)^2 \tag{20}$$

With adaptations represented as a diffusive flux, many populations with extremely low abundances can rapidly emerge across the trait space in just a few time steps. Aside from increasing the computational load of the model, the proliferation of traits by numerical diffusion may also lead to the emergence of populations with traits far removed from those already established in the system. As our goal is to model the emergence of phenotypes by descent from established populations, we prevent trait diffusion at low biomasses in two ways. First, we scale the growth and grazing rates by a function that decreases rapidly towards zero as a population's biomass falls below a functional extinction threshold, ϵ.

$$\vec{\gamma}_\epsilon = 1 - \mathrm{e}^{-\vec{B}/\epsilon} \tag{21}$$

This factor is applied to growth and grazing as follows,

$$\vec{\mu} = \frac{\vec{\mu}_{max} \cdot \vec{\alpha} \cdot P}{\vec{\mu}_{max} + \vec{\alpha} \cdot P} \cdot \gamma \cdot \vec{\gamma}_\epsilon \tag{22}$$

and

$$\vec{G}^+ = \vec{g}' \cdot \left(\boldsymbol{\phi}^{\mathrm{T}} \vec{B}\right) \cdot \vec{\gamma}_\epsilon \tag{23}$$

$$\vec{G}^- = \boldsymbol{\phi}\left(\vec{B} \cdot \vec{g}'\right) \cdot \vec{\gamma}_\epsilon \tag{24}$$

Secondly, we add an additional mortality term that becomes large as a population's biomass falls below ϵ.

$$\vec{\delta}_\epsilon = 10 \cdot \mathrm{e}^{-\vec{B}/\epsilon} \tag{25}$$

This function is incorporated into equation 16, such that

$$\frac{d\vec{B}}{dt} = \left(\vec{\mu} + \lambda \cdot \vec{G}^+ - \vec{G}^- - (1 + B)\delta - \vec{\delta}_\epsilon\right) \cdot \vec{B} + \vec{L}_e \tag{26}$$

These modifications prevent the growth of populations at unrealistically low abundances. Functionally extinct populations can only recover when their biomass is raised back above ϵ by mutation from adjacent phenotypes in the trait space.

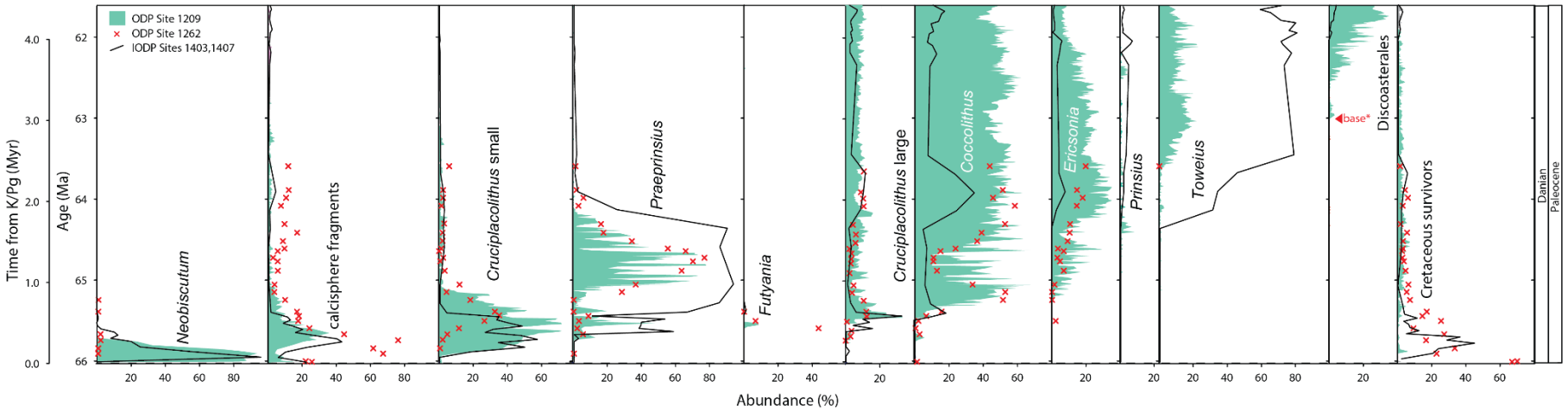

Figure S1. Relative abundance of key nannoplankton groups forming a succession of abundance peaks ('acmes'). Data from ODP Site 1209 (Shatsky Rise, equatorial Pacific), ODP Site 1262 (Walvis Ridge, South Atlantic) and IODP Site 1403 and 1407 (Newfoundland Ridge, North Atlantic), and ordered by stratigraphic appearance in ODP Site 1209. Cretaceous survivor taxa comprise mostly *Zeugrhabdotus*, *Cyclagelosphaera*, *Markalius*, *Neocrepidolithus* (diploid phase coccoliths) and holococcoliths (haploid phase coccoliths). Data from ODP Site 1262 extends up to 63.2 Ma (~+2.5 Ma post extinction event). Age models are detailed in Material and Methods (*24*). The genus *Cruciplacolithus* has been split into smaller and larger taxa (approximating to *Cr. primus* and *Cr. intermedius* + *Cr. asymmetricus*, respectively) using coccolith length data (*24*).

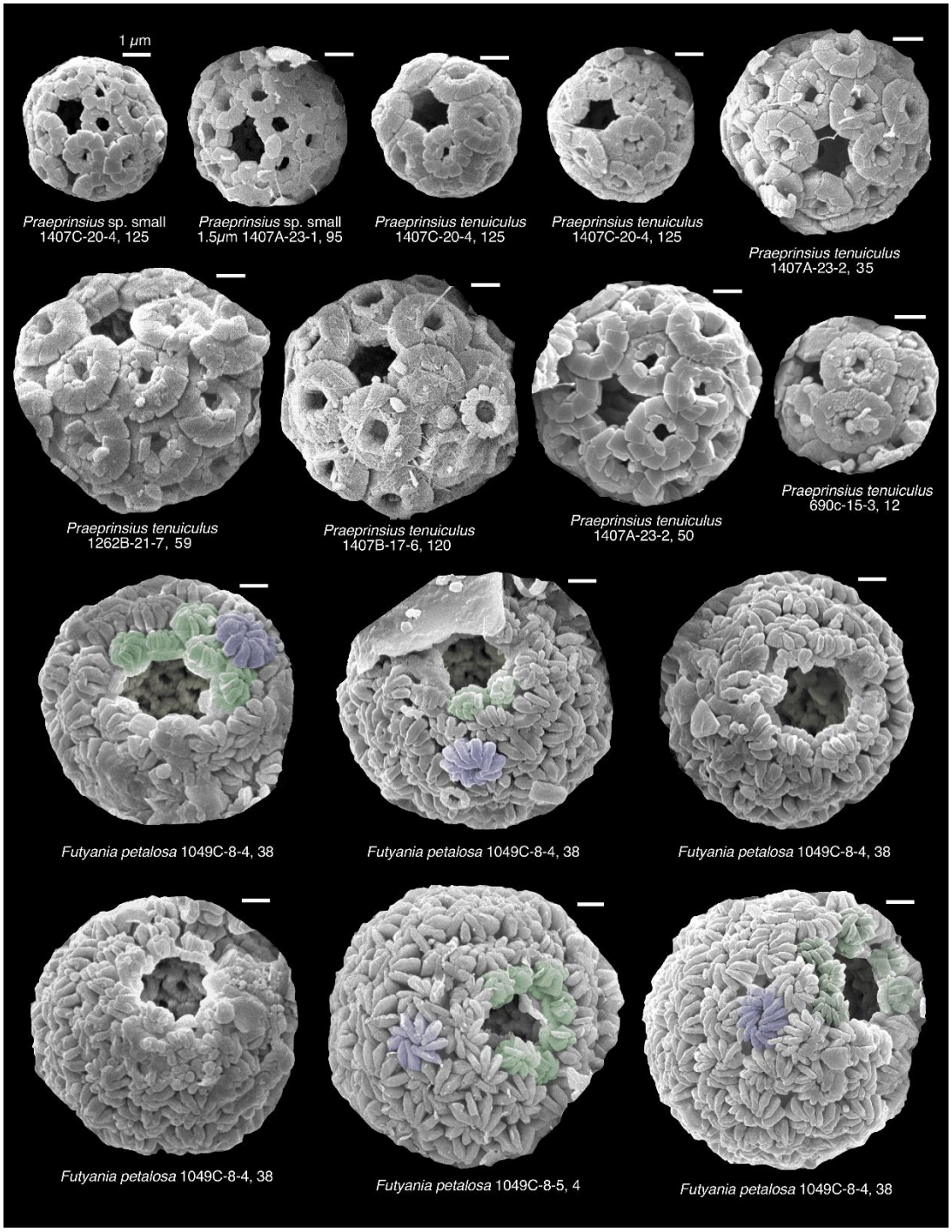

Figure S2a. Scanning electron microscope images of coccospheres with flagellar openings. The upper nine images are *Praeprinsius* specimens and the lower six are *Futyania,* which additionally display modified circum-flagellar coccoliths (i.e., coccoliths with a different morphology around the opening to those on the rest of the coccosphere, shaded in green for comparison with example non-circum-flagellar coccoliths highlighted in purple). For site and sample details see tables S1 and S2.

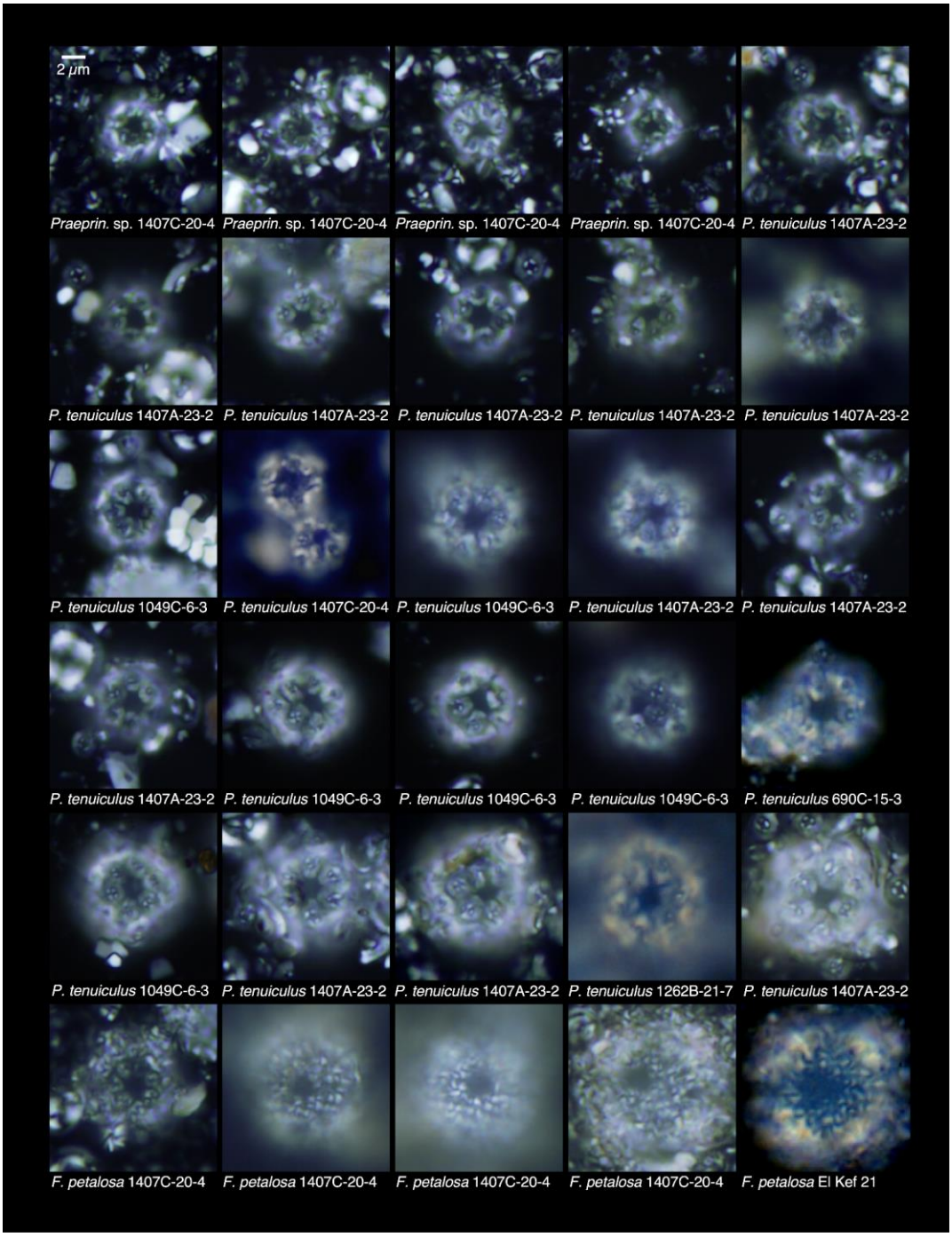

Figure S2b. Light microscope images of coccospheres with flagellar openings. The majority of the images are *Praeprinsius* specimens but the images in the lowermost row are *Futyania*. Full sample identifiers: 1407C 20-4, 125 cm; 1407A-23-2, 50 cm; 1049C-6-3, 1262B 21-7, 59 cm, 145 cm. For site and sample details see tables S1 and S2.

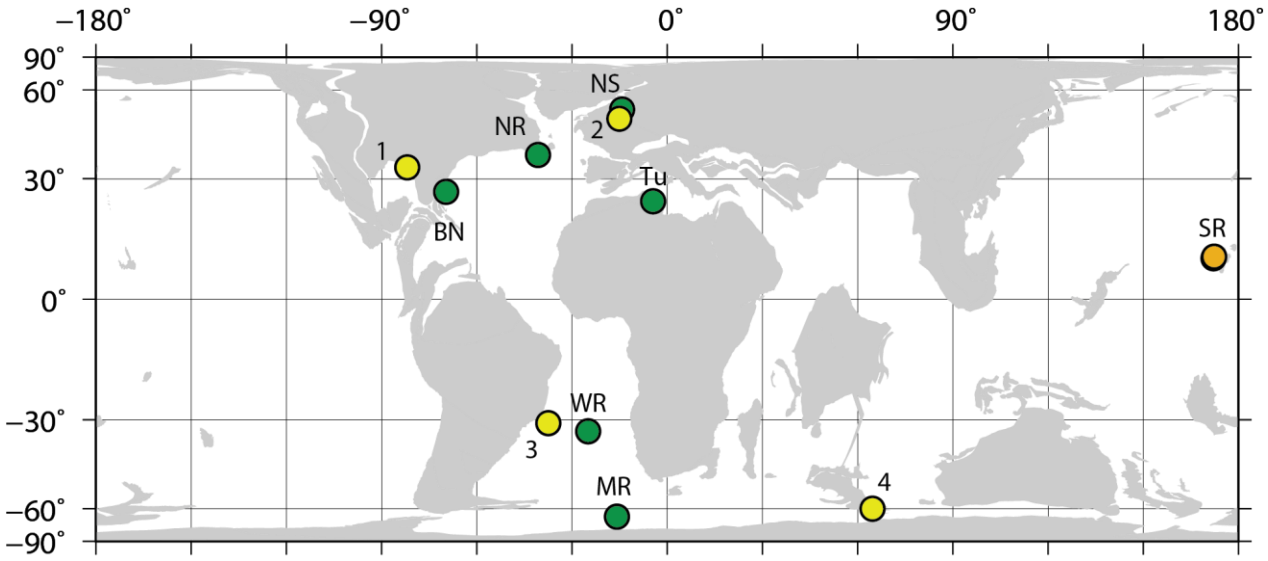

Figure S3. Location of sites used in this study. NR – Newfoundland Ridge (IODP Sites 1403 and 1407), BN – Blake Nose (ODP Site 1049), WR – Walvis Ridge (ODP Site 1262), MR – Maud Rise (ODP Site 690), SR – Shatsky Rise (ODP Site 1209 and 1210), Tu – Tunisia (El Kef outcrop) and NS – North Sea (proprietary well sample, see table S2). Sites marked as green are those from which we have coccospheres (see table S1), SR is marked in orange because we only have assemblage data and not coccosphere information from this site. In yellow are sites where published images of coccospheres show flagellar openings: 1. West Alabama (*37*), 2. Geulhemmerberg (Netherlands, ref. *38*), 3. DSDP Site 356, Sao Paulo Plateau (*39*) and 4. ODP Site 738, Kerguelen Plateau, Indian Ocean sector of the Southern Ocean (*40*). Location and dataset details in tables S1 and S2. The basemap is a 66 Ma reconstruction from the ODSN website (www.odsn.de).

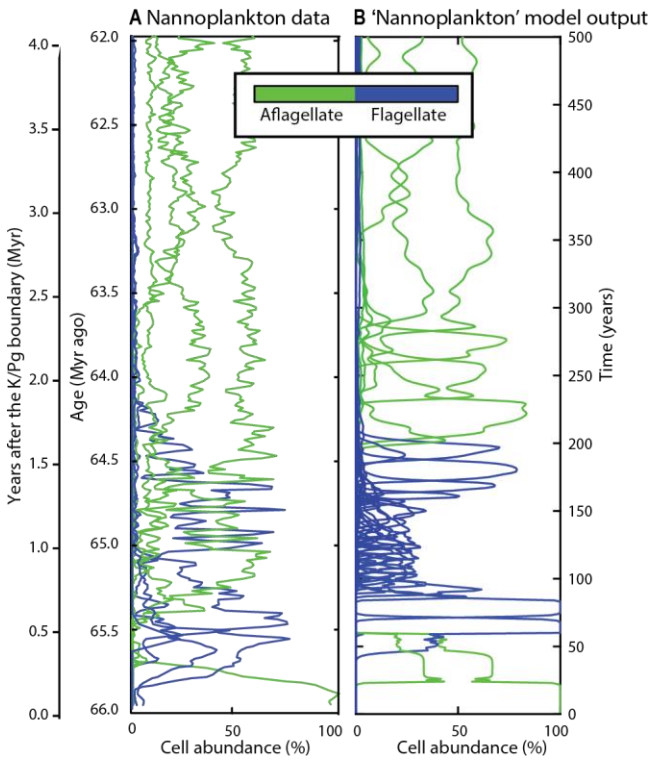

Figure S4. Taxon-specific abundance data differentiated according to the presence of flagellar openings and degree of heterotrophy. (**A**) shows the abundances of different Danian taxa (from ODP Site 1209, sub-equatorial Pacific) color-coded according to whether their cells are flagellate (or considered mixotrophic) or not, blue and green, respectively. (**B**) shows modelled abundances of 'species' in the nannoplankton size range (2-20 microns) again color-coded according to whether the cells are flagellate. Note that mutation and evolution proceed much faster in the model because the model applies a simplified 'trait diffusion' approach to evolution (*24*).

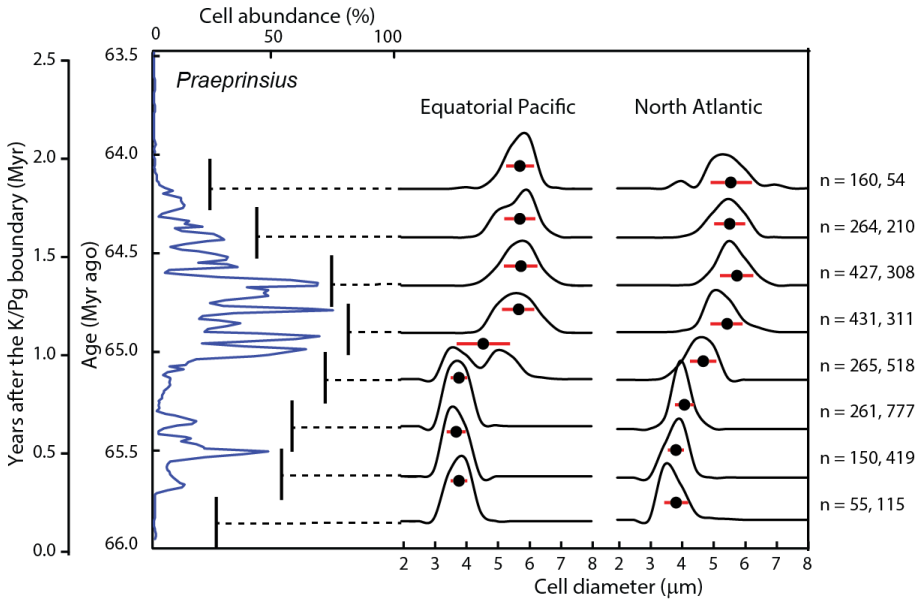

Figure S5. Morphological variation across the early Danian taxon *Praeprinsius.* Data from ODP Site 1209 (Equatorial Pacific) and IODP Sites 1403 plus 1407 (North Atlantic). On the left is the percent abundance of *Praeprinsius* in cell numbers relative to total calcareous nannoplankton fossils, using high-resolution coccolith abundance data (converted to cell numbers) (*24*) from ODP Site 1209 (original coccolith data from *9*). The vertical black lines indicate the time slices across which length measurements of individual coccoliths have been measured and integrated to produce the frequency plots (black histograms) of size on the right-hand side; these time slices are the same for the two sites. The black filled-in circle under each histogram indicates mean cell size and the red line shows one standard deviation either side of the mean. Number of liths measured per time slice per site is given as the n number for ODP Site 1209 and IODP Sites 1403 plus 1407, respectively. Coccolith length measurements have been converted to an estimate of the average cell size associated with coccoliths of this length via the conversion: cell size = 1.447coccolith length + 1.14. This conversion is based on measurements of 147 whole coccospheres and the coccoliths that form these coccospheres from samples that span the duration of the *Praeprinsius* acme from ODP Sites 1209, 1403 and 1407 (*25*). The similarity in means and trends in size across the two regions suggests global evolutionary size increases across *Praeprinsius*.

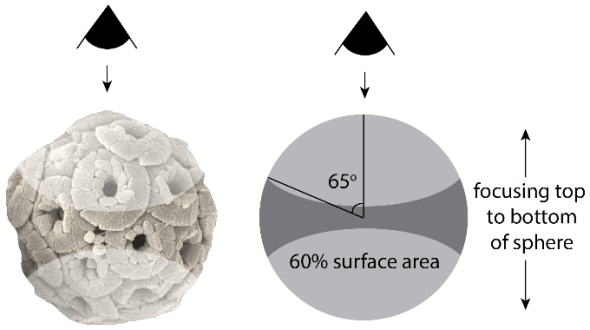

Figure S6. Illustration of spherical cap calculations. Under light microscope observation, the equatorial region of coccospheres is obscured and therefore only part of the area of the sphere can be observed clearly to assess for presence of coccosphere openings. We estimate that we can typically observe a part of the sphere corresponding to the pole of each coccosphere to about 65 degrees in the upper and lower hemispheres, correspond to 60% of the surface area.

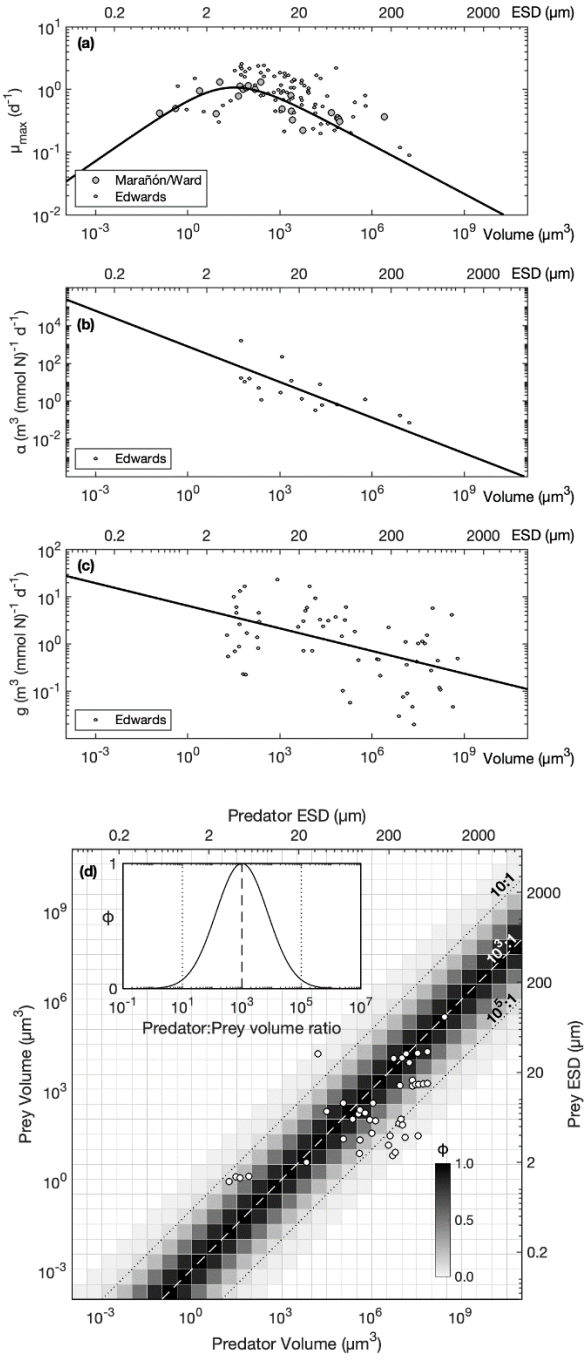

Figure S7. Size-dependent ecophysiological parameters: (a) maximum growth rate, $\boldsymbol{\mu_{max}}$ (*64, 77, 80*); (b) nitrate affinity, $\boldsymbol{\alpha}$ (*64*); (c) grazing clearance rate, $\boldsymbol{g}$ (*62*); (d) predator-prey size-ratio-dependent capture efficiency, $\boldsymbol{\phi}$ (*63*).

Site	Sample identifier	Age (Ma) and age model	Kyrs post event	Sample depth	Coccospheres observed: Taxa recorded with flagellar openings (% of coccospheres exhibiting openings)	Coccospheres observed: Taxa recorded with no flagellar openings
Newfoundland Ridge	1407A 22-3, 80cm	61.933*	4089	208.25 rmcd	None	*Toweius*
(North Atlantic)	1407A 22-4, 80 cm	62.073*	3949	209.75 rmcd	None	*Toweius*
	1407A 22-5, 60 cm	62.333*	3689	211.05 rmcd	None	*Toweius*
	1407A-23-1, 5 cm	63.438*	2584	212.49 rmcd	***Praeprinsius*** (61%), *Prinsius* (40%)	*Biscutum, Cocc., Cruci., Erics.,* early *Toweius,*
	1407A 23-1, 95 cm	64.128*	1894	213.39 rmcd	***Praeprinsius*** (62%)	*Coccolithus, Cruciplacolithus*
	1407A 23-2, 35 cm	64.506*	1526	214.29 rmcd	*Praeprinsius* (52%)	*Coccolithus, Cruciplacolithus*
	1407A 23-2, 50cm	64.607*	1415	214.44 rmcd	***Praeprinsius*** (60%)	No other coccospheres found
	1407A 23-2, 75 cm	64.776*	1246	214.69 rmcd	***Praeprinsius*** (62%)	*Coccolithus*
	1407C 20-4, 125 cm	*Futyania* acme, ~65.55†	~270	214.13 mcd	*Futyania* (57%), *Praeprinsius* (47%)	*Coccolithus, Cruciplacolithus, Watznaueria*
	1403A 26-2, 20 cm	65.061**	961	243.28 mcd	uncommon *Praeprinsius*	*Coccolithus, Cruci., Watznaueria, Markalius*
	1403A 26-4, 74 cm	65.744**	278	246.82 mcd	None	*Coccolithus*
	1403A 26-4, 138 cm	65.943**	79	247.46 mcd	None	*Neobiscutum, Watznaueria*
Blake Nose	1049C 6-3, 99 cm	*Praepr.* acme, ~64.75†	~1270	94.01 mbsf	***Praeprinsius*** (62%)	*Braarudosphaera*
(Central Atlantic)	1049C 6-3, 145 cm	*Praepr.* acme, ~64.75†	~1270	94.47 mbsf	***Praeprinsius*** (65%)	*Braarudosphaera*
	1049C 7-1, 115 cm	*Praepr.* acme, ~64.75†	~1270	97.67 mbsf	***Praeprinsius*** (68%)	*Coccolithus*
	1049C 8-4, 38 cm	base *Futyania* acme, very top of the *Neobisc.* acme, ~65.55†	~270	111.00 mbsf	***Futyania*** (<u>46%</u>)	No other coccospheres found
	1049C 8-4, 146 cm		~270	112.08 mbsf	***Futyania*** (87%)	*Braarudosphaera*
	1049C 8-5, 4 cm		~270	112.16 mbsf	***Futyania* (61%), *Praeprinsius*** (71%)	*Braarudosphaera*
El Kef	El Kef 11	*Neobisc.* acme, ~65.90†	~120	11 m	None	*Neobiscutum, Biscutum*
(North Africa)	El Kef 13	*Neobisc.* acme, ~65.90†	~120	13 m	None	*Neobiscutum, Braarudosphaera*
	El Kef 21	*Futyania* acme, ~65.55†	~270	21 m	***Futyania*** (64%), ?*Praeprinsius*	*Cruciplacolithus*
Walvis Ridge (Sth Atl.)	1262B 21-H7, 59 cm	64.724‡	1298	210.44 mcd	*Praeprinsius* (55%)	*Cyclagelosphaera*
Maud Rise (Southern Ocean)	690C 15x-3, 12 cm	towards base of *Praepr.* acme, ~65.2†	~820	246.04 mbsf	*Praeprinsius* (35%)	No other coccospheres found
North Sea (Europe)	Proprietary well material, no depth information available				single specimen of *Prinsius* imaged and shown in Fig. 2	
Published SEM images:						
Kerguelen Plateau (Southern Ocean)					*Prinsius dimorphous,* Ref. *90,* Pl. 1, fig. 4	
Sao Paul Plateau (South Atlantic)					*Prinsius dimorphous* , Ref. *89,* Pl. 4, fig. 1	
Geulhemmerberg (Netherlands, Europe)					*Futyania,* Ref. *61,* Pl. 6, fig. 4	
Alabama (Gulf Coast, USA)					*Futyania,* Ref. *88,* Pl. 1, fig. 4	

Table S1. Coccosphere observations by age and site. Underlined percentages are from SEM observations where only ~30-50% of the coccosphere surface can be seen clearly enough to assess presence of an opening. The rest are from LM observations where ~60% of the coccosphere surface can be seen clearly enough to assess presence of an opening (*24*) (see fig. S6). Taxa in bold indicate percent abundances of coccosphere openings which indicate that all individuals in the populations have openings. The thresholds are 30% in SEM and 60% under LM observation. The bottom four sites are ones for which images have been published that exhibit flagellar openings. *Neobisc. – Neobiscutum; Praepr. – Praeprinsius; Cruci. – Cruciplacolithus; Cocc. – Coccolithus; Erics. – Ericsonia*. Depths: mcd - meters composite depth; rmcd – revised meters composite depth; mbsf – meters below seafloor; El Kef m – meters above K/Pg boundary. Age models: *Biostratigraphy (shipboard, ref. *54*, and more recent revision herein); **ref *2*, based on cyclostratigraphy; †based on biostratigraphy (herein) and position of chron C29N/C29R boundary at 247.55 mbsf (*83*); ‡ref. *52* based on cyclostratigraphy. All ages use the Geological Timescale 2012 (GTS2012, *84*).

Location name	Shatsky Rise (SR)	Newfoundland Ridge (NR)	Blake Nose (BN)	Tunisia (Tu)	Walvis Ridge (WR)	Maud Rise (MR)
Region	Northwest Pacific	North Atlantic	Central Atlantic	Onshore North Africa	South Atlantic	Southern Ocean
Drill/core site identifier	ODP Sites 1209A,B,C, 1210A	IODP Sites 1403A; 1407A,C	ODP Site 1049C	El Kef core	ODP Site 1262B	ODP Site 690C
Present water depth (meters)	2387 (Site 1209) 2574 (Site 1210)	4949 (Site 1403) 3073 (Site 1407)	2670 m	N/A	4759 m	2914 m
Paleo-water depth at K/Pg	Bathyal	Lower bathyal	Lower bathyal	Shallow, neritic	Abyssal	Lower to middle bathyal
Today's setting	Oceanic rise flank	Oceanic abyssal ridge	Base of slope	Onshore	Base of oceanic abyssal ridge	Oceanic ridge flank
Paleo-environment	Open-ocean, gyre, sub-equatorial	Open-ocean, mid latitude	Open-ocean with some shelf influence, sub-tropical	Neritic, tropical	Open-ocean, mid latitude	Open-ocean, high latitude
Preservation state†	Moderate to good	Good to excellent	Good to excellent	Good to excellent	Moderate to excellent	Moderate to excellent
Type of data utilised herein:						
diversity and taxon abundances from coccoliths	✓*	✓			✓	
length mesurements of coccoliths	✓	✓				
coccosphere measurements and observations		✓**	✓	✓	✓	✓

Table S2. Summary of main locations and datasets used in the study. *Diversity and taxon abundance data published in ref *9*. **Some coccosphere measurements utilized in ref *9* to produce their estimated average cell volume. †Based on our assessment herein (*24*). References for SR – *9, 19*; NR – *2, 54*; BN – *85*; Tu – *15, 18*; WR – *10, 12, 54*; MR – *18*. The single specimen of *Prinsius* imaged in Figure 2 from the North Sea is from Danian material from a proprietary well sample and therefore we are unable to provide additional information. See location map (fig. S3) for paleogeography.

Early Danian (pre 64.20 Myrs) compared with:	Late Cretaceous		later Danian (post 64.20 Myrs)	
	Shatsky Rise, Sub-equ. Pacific	Walvis Ridge, South Atlantic	Shatsky Rise, Sub-equ. Pacific	Newfoundland Ridge, North Atlantic
mean (%):	57.33, 26.92	59.62, 44.26	53.69, 8.44	78.13, 3.18
SD:	28.02, 4.95	18.10, 3.74	27.00, 8.92	10.45, 4.28
df:	48	12	102	14
t:	7.88	-3.05	14.61	21.97
p (critical two tail):	<<0.0001	0.01	<<0.0001	<<0.0001

Table S3. Paired-sample t-test results of flagellate communities through time. Comparison of percent flagellate cells (here using percent coccoliths) in the ealry Danian (acme phase up to 64.20 Ma) with the latest Cretaceous and the later Danian (post 64.20 Ma). Comparisons have only been made between populations at the same location. For Shatsky Rise (ODP Sites 1209 and 1210), we are able to directly compare coccolith abundance data from the early Danian with both the Late Cretaceous and the later Danian. For Walvis Ridge, we only have data allowing comparison of early Danian abundances with the Late Cretaceous, and for Newfoundland Ridge, only with the later Danian (*24*). For the mean, the first value given corresponds to the mean % flagellate abundance for the early Danian interval. The second value is the mean of the interval the early Danian is being compared with. The tests demonstrate that the interval up to approximately 64.2 Ma with unusually high levels of mixotrophic cells, is statistically distinct from either the preceding Late Cretaceous communities or the subsequent later Danian. SD – standard deviation, df – degrees of freedom, t – t value, p – p value.

Parameter	Symbol	Coefficient (a)	Exponent (b)	Units
Biomass-specific P affinity	α	794	-0.63	m^3 (mmol N)$^{-1}$ d^{-1}
Biomass-specific grazing clearance rate	g	6.48	-0.16	m^3 (mmol N)$^{-1}$ d^{-1}
Maximum population growth rate	μ_{max}	*See equation* 7		d^{-1}
Theoretical growth rate at infinite quota	μ^{∞}	4.70	-0.26	d^{-1}
Maximum cellular N uptake rate	ρ_{max}	0.024	1.10	mmol N cell^{-1} d^{-1}
Minimum cellular N quota	Q_{min}	0.032	0.76	mmol N cell^{-1}

Table S4a. Size-dependent parameters with allometric scaling coefficients reported in the literature (*64, 77, 62*). The size-dependent value of each parameter, p, is given by $p = a\left(\frac{V}{V_1}\right)^b$, where V is the cell volume and V_1 is a normalisation constant of 1 μm^3. Note that μ^{∞}, ρ_{max} and Q_{min} are only used to constrain μ_{max} in equation 7.

Parameter	Symbol	Value	Units
Basal mortality rate	δ	0.1	d^{-1}
Optimal predator:prey volume ratio	ϑ_{opt}	1000	-
Breadth of prey kernel	ϕ_{σ}	2	-
Grazing assimilation efficiency	λ	0.7	-
Prey refuge coefficient	Λ	-100	(mmol N)$^{-1}$
Fraction of growth to adjacent phenotypes	σ	10^{-15}	-
Trophic trade-off parameter	τ	1	-
Light-limitation factor	γ	0.1	
Incoming nutrient concentration	N_0	5	mmol N m^{-3}
Incoming flow rate	κ	0.01	d^{-1}

Table S4b. Size-independent parameters.

REFERENCES AND NOTES

1. P. Schulte, L. Alegret, I. Arenillas, J. A. Arz, P. J. Barton, P. R. Bown, T. J. Bralower, G. L. Christeson, P. Claeys, C. S. Cockell, G. S. Collins, A. Deutsch, T. J. Goldin, K. Goto, J. M. Grajales-Nishimura, R. A. F. Grieve, S. P. S. Gulick, K. R. Johnson, W. Kiessling, C. Koeberl, D. A. Kring, K. G. MacLeod, T. Matsui, J. Melosh, A. Montanari, J. V. Morgan, C. Neal, D. J. Nichols, R. D. Norris, E. Pierazzo, G. Ravizza, M. Rebolledo-Vieyra, W. U. Reimold, E. Robin, T. Salge, R. P. Speijer, A. R. Sweet, J. Urrutia-Fucugauchi, V. Vajda, M. T. Whalen, P. S. Willumsen, The Chicxulub asteroid impact and mass extinction at the Cretaceous-Paleogene boundary. *Science* **327**, 1214–1218 (2010).

2. P. M. Hull, A. Bornemann, D. E. Penman, M. J. Henehan, R. D. Norris, P. A. Wilson, P. Blum, L. Alegret, S. J. Batenburg, P. R. Bown, T. J. Bralower, C. Cournede, A. Deutsch, B. Donner, O. Friedrich, S. Jehle, H. Kim, D. Kroon, P. C. Lippert, D. Loroch, I. Moebius, K. Moriya, D. J. Peppe, G. E. Ravizza, U. Röhl, J. D. Schueth, J. Sepúlveda, P. F. Sexton, E. C. Sibert, K. K. Śliwińska, R. E. Summons, E. Thomas, T. Westerhold, J. H. Whiteside, T. Yamaguchi, J. C. Zachos, On impact and volcanism across the Cretaceous-Paleogene boundary. *Science* **367**, 266–272 (2020).

3. S. P. S. Gulick, T. J. Bralower, J. Ormö, B. Hall, K. Grice, B. Schaefer, S. Lyons, K. H. Freeman, J. V. Morgan, N. Artemieva, P. Kaskes, S. J. de Graaff, M. T. Whalen, G. S. Collins, S. M. Tikoo, C. Verhagen, G. L. Christeson, P. Claeys, M. J. L. Coolen, S. Goderis, K. Goto, R. A. F. Grieve, N. M. Call, G. R. Osinski, A. S. P. Rae, U. Riller, J. Smit, V. Vajda, A. Wittmann; Expedition 364 Scientists, The first day of the Cenozoic. *Proc. Natl. Acad. Sci. U.S.A.* **116**, 19342–19351 (2019).

4. S. D'Hondt, Consequences of the Cretaceous/Paleogene mass extinction for marine ecosystems. *Annu. Rev. Ecol. Evol. Syst.* **36**, 295–317 (2005).

5. K. Kaiho, N. Oshima, K. Adachi, Y. Adachi, T. Mizukami, M. Fujibayashi, R. Saito, Global climate change driven by soot at the K-Pg boundary as the cause of the mass extinction. *Sci. Rep.* **6**, 28427 (2016).

6. C. G. Bardeen, R. R. Garcia, O. B. Toon, A. J. Conley, On transient climate change at the Cretaceous−Paleogene boundary due to atmospheric soot injections. *Proc. Natl. Acad. Sci. U.S.A.* **114**, E7415–E7424 (2017).

7. M. J. Henehan, A. Ridgwell, E. Thomas, S. Zhang, L. Alegret, D. N. Schmidt, J. W. B. Rae, J. D. Witts, N. H. Landman, S. E. Greene, B. T. Huber, J. R. Super, N. J. Planavsky, P. M. Hull, Rapid ocean acidification and protracted Earth system recovery followed the end-Cretaceous Chicxulub impact, *Proc. Natl. Acad. Sci. U.S.A.* **116**, 22500–22504 (2019).

8. P. R. Bown, J. A. Lees, J. R. Young, Calcareous nannoplankton evolution and diversity through time, in *Coccolithophores–From Molecular Processes to Global Impacts*, H. Thierstein, J. R. Young, Eds. (Springer, 2004), pp. 481–508.

9. S. A. Alvarez, S. J. Gibbs, P. R. Bown, H. Kim, R. M. Sheward, A. Ridgwell, Diversity decoupled from ecosystem function and resilience during mass extinction recovery. *Nature* **574**, 242–245 (2019).

10. H. S. Birch, H. K. Coxall, P. N. Pearson, D. Kroon, D. N. Schmidt, Partial collapse of the marine carbon pump after the Cretaceous-Paleogene boundary. *Geology* **44**, 287–290 (2016).

11. M. J. Henehan, P. M. Hull, D. E. Penman, J. W. B. Rae, D. N. Schmidt, Biogeochemical significance of pelagic ecosystem function: An end-Cretaceous case study. *Philos. Trans. R. Soc. B* **371**, 20150510 (2016).

12. L. Alegret, E. Thomas, Deep-Sea environments across the Cretaceous/Paleogene boundary in the eastern South Atlantic Ocean (ODP Leg 208, Walvis Ridge). *Mar. Micropaleontol.* **64**, 1–17 (2007).

13. J. Sepúlveda, J. E. Wendler, E. Summons, Roger, K.-U. Hinrichs, Rapid resurgence of marine productivity after the Cretaceous-Paleogene mass extinction. *Science* **326**, 129–132 (2009).

14. B. Schaefer, K. Grice, M. J. L. Coolen, R. E. Summons, X. Cui, T. Bauersachs, L. Schwark, M. E. Böttcher, T. J. Bralower, S. L. Lyons, K. H. Freeman, C. S. Cockell, S. P. S. Gulick, J. V. Morgan, M. T. Whalen, C. M. Lowery, V. Vajda, Microbial life in the nascent Chicxulub crater. *Geology* **48,** 328–332 (2020).

15. H. Brinkhuis, H. Leereveld, Dinoflagellate cysts from the Cretaceous/Tertiary boundary sequence of El Kef, northwest Tunisia. *Rev. Palaeobot. Palynol.* **56**, 5–19 (1988).

16. P. A. Sims, D. G. Mann, L. K. Medlin, Evolution of the diatoms: Insights from fossil, biological and molecular data. *Phycologia* **45**, 361–402 (2006).

17. S. Ribeiro, T. Berge, N. Lumdholm, T. J. Andersen, F. Abrantes, M. Ellegaard, Phytoplankton growth after a century of dormancy illuminates past resilience to catastrophic darkness. *Nat. Commun.* **2**, 311 (2011).

18. J. J. Pospichal, Calcareous nannoplankton mass extinction at the Cretaceous/Tertiary boundary: An update, in *The Cretaceous-Tertiary Event and Other Catastrophes in Earth History*, G. Ryder, D. E. Fastovsky, S. Gartner, Eds. (GSA Special Paper 307, Geological Society of America, 1996), pp. 335–360.

19. P. Bown, Selective calcareous nannoplankton survivorship at the Cretaceous-Tertiary boundary. *Geology* **33**, 653–656 (2005).

20. A. Houdan, I. Probert, C. Zatylny, B. Vérnon, C. Billard, Ecology of oceanic coccolithophores. I. Nutritional preferences of the two stages in the life cycle of *Coccolithus braarudii* and *Calcidiscus leptoporus. Aquat. Microb. Ecol.* **44**, 291–301 (2006).

21. L. Cros, M. Estrada, Holo-heterococcolithophore life cycles: Ecological implications. *Mar. Ecol. Prog. Ser.* **492**, 57–68 (2013).

22. A. Winter, R. W. Jordan, P. H. Roth, Biogeography of living coccolithophores in ocean waters, in *Coccolithophores*, A. Winter, W. G. Siesser, Eds. (Cambridge Univ. Press, 1994), pp. 161–178.

23. J. Godrijan, J. R. Young, D. Marić Pfannkuchen, R. Precali, M. Pfannkuchen, Coastal zones as important habitats of coccolithophores: A study of species diversity, succession, and life-cycle phases. *Limnol. Oceanogr.* **63**, 1692–1710 (2018).

24. Materials and Methods are available as the Supplementary Materials.

25. H. L. Jones, B. S. C. Leadbeater, J. C. Green, Mixotrophy in haptophytes, in *The Haptophyte Algae*, J. C. Green, B. S. C. Leadbeater, Eds. (Systematics Association Special, Clarendon Press, 1994), vol. **51**, pp. 247–263.

26. J. Dölger, L. T. Nielsen, T. Kiørboe, A. Andersen. Swimming and feeding of mixotrophic biflagellates. *Sci. Rep.* **7**, 39892 (2017).

27. J. R. Young, P. R. Bown, J. A. Lees, Nannotax3 website (2020); www.mikrotax.org/Nannotax3/.

28. M. Kawachi, I. Inouye, Functional roles of the haptonema and the spine scales in the feeding process of *Chrysochromulina spinifera* (Fournier) Pienaar et Norris (Haptophyta = Prymnesiophyta). *Phycologia* **34**, 193–200 (1995)

29. W. Eikrem, L. K. Medlin, J. Henderiks, S. Rokitta, B. Rost, I. Probert, J. Throndsen, B. Edvardsen, Haptophytes, in *Handbook of the Protists*, J. M. Archibald A. G. B. Simpson, C. H. Slamovits, L. Margulis, Eds. (Springer, 2016), pp. 1–59.

30. R. A. DePalma, J. Smit, D. A. Burnham, K. Kuiper, P. L. Manning, A. Oleinik, P. Larson, F. J. Maurrasse, J. Vellekoop, M. A. Richards, L. Gurche, W. Alvarez, A seismically induced onshore surge deposit at the KPg boundary, North Dakota. *Proc. Natl. Acad. Sci. U.S.A.* **116**, 8190–8199 (2019).

31. L. K. Medlin, A. G. Sáez, J. R. Young, A molecular clock for coccolithophores and implications for selectivity of phytoplankton extinctions across the K/T boundary. *Mar. Micropal.* **67**, 69–86 (2008).

32. F. Unrein, J. M. Gasol, F. Not, I. Forn, R. Massana, Mixotrophic haptophytes are key bacterial grazers in oligotrophic coastal waters. *ISME J.* **8**, 164–176 (2014).

33. J. M. Burkholder, P. M. Glibert, H. M. Skelton, Mixotrophy, a major mode of nutrition for harmful algal species in eutrophic waters. *Harmful Algae* **8**, 77–93 (2008).

34. D. K. Stoecker, P. J. Lavrentyev, Mixotrophic plankton in the polar seas: A pan-arctic review. *Front. Mar. Sci.* **5**, 292 (2018).

35. D. H. Erwin, The end and the beginning: Recoveries from mass extinctions. *Trends Evol. Ecol.* **13**, 344–349 (1998).

36. D. P. G. Bond, S. E. Grasby, On the causes of mass extinctions. *Palaeogeogr. Palaeoclimatol. Palaeoecol.* **478**, 3–29 (2017).

37. C. H. Ellis, W. H. Lohmann, Toweius petalosus new species, a Paleocene calcareous nannofossil from Alabama. *Tulane Stud. Geol. Paleontol.* **10**, 107–110 (1973).

38. H. Mai, New coccolithophorid taxa from Geulhemmerberg airshaft, lower Paleocene, The Netherlands. *Micropaleontology* **47**, 144–154 (2001).

39. H. Mai, T. Hildebrand-Habel, K. von Salis Perch-Nielsen, H. Willems, Paleocene coccospheres from DSDP Leg 39, Site 356, São Paulo Plateau, S Atlantic Ocean. *J. Nannoplankton Res.* **20**, 21–29 (1998).

40. W. Wei, J. J. Pospichal, Danian calcareous nannofossil succession at ODP Site 738 in the southern Indian Ocean. *Proc. ODP Sci. Results* **119**, 495–512 (1991); doi:10.2973/odp.proc.sr.119.154.1991.

41. P. R. Bown, J. R. Young, Techniques, in *Calcareous Nannofossil Biostratigraphy*, P. R. Bown, Ed. (Kluwer Academic Publishers, 1998), pp. 16–28.

42. P. R. Bown, T. Dunkley Jones, J. A. Lees, P. N. Pearson, J. R. Young, R. Randell, H. K. Coxall, J. Mizzi, C. J. Nicholas, A. Karega, J. Singano, B. S. Wade, A Paleogene calcareous microfossil Konservat-Lagerstätte from the Kilwa Group of coastal Tanzania. *Geol. Soc. Am. Bull.* **120**, 3–12 (2008).

43. J. A. Lees, P. R. Bown, J. R. Young, J. B. Riding, Evidence for annual records of phytoplankton productivity in the Kimmeridge Clay Formation coccolith stone bands (Upper Jurassic, Dorset, UK). *Mar. Micropaleontol.* **52**, 29–49 (2004).

44. L. Šupraha, Z. Ljubešić, H. Mihanović, J. Henderiks, Observations on the life cycle and ecology of *Acanthoica quattrospina* Lohmann from a Mediterranean estuary. *J. Nannoplankton Res.* **34**, 49–56 (2014).

45. M. Kawachi, I. Inouye, Observations on the Flagellar Apparatus of a Coccolithophorid, *Cruciplacolithus neohelis* (Prymnesiophyceae). *J. Plant Res.* **107**, 53–62 (1994).

46. H. J. Jeong, Y. Du Yoo**,** J. Y. Park, J. Y. Song, S. T. Kim, S. H. Lee, K. Y. Kim, W. H. Yih, Feeding by phototrophic red-tide dinoflagellates: Five species newly revealed and six species previously known to be mixotrophic. *Aquat. Microb. Ecol.* **40**, 133–150 (2005).

47. Y. Du Yoo, H. J. Jeong, M. S. Kim, N. S. Kang, J. Y. Song, W. Shin, K. Y. Kim, K. Lee, Feeding by phototrophic red-tide dinoflagellates on the ubiquitous marine diatom *Skeletonema costatum*. *J. Eukaryot. Microbiol.* **56**, 413–420 (2009).

48. S. J. Gibbs, P. R. Bown, B. H. Murphy, A. Sluijs, K. M. Edgar, H. Pälike, C. T. Bolton, J. C. Zachos, Scaled biotic disruption during early Eocene global warming events. *Biogeosciences* **9**, 4679–4688 (2012).

49. K. Perch-Nielsen, Cenozoic calcareous nannofossils, in *Plankton Stratigraphy*, H. M. Bolli, J. B. Saunders, K. Perch-Nielsen, Eds. (Cambridge Univ. Press, 1985), pp. 427–554.

50. P. R. Bown, Paleocene calcareous nannofossils from Tanzania (TDP sites 19, 27 and 38). *J. Nannoplankton Res.* **36**, 1–32 (2016); http://ina.tmsoc.org/JNR/JNRcontents.htm.

51. T. Westerhold, U. Röhl, I. Raffi, E. Fornaciari, S. Monechi, V. Reale, J. Bowles, H. F. Evans, Astronomical calibration of the Paleocene time. *Palaeogeogr. Palaeoclimatol. Palaeoecol.* **257**, 377–403 (2008).

52. J. Dinarès-Turell, T. Westerhold, V. Pujalte, U. Röhl, D. Kroon, Astronomical calibration of the Danian stage (Early Paleocene) revisited: Settling chronologies of sedimentary records across the Atlantic and Pacific Oceans. *Earth Planet. Sci. Lett.* **405**, 119–131 (2014).

53. T. Westerhold, U. Röhl, B. Donner, J. C. Zachos, Global extent of early Eocene hyperthermal events: A new Pacific benthic foraminiferal isotope record from Shatsky Rise (ODP Site 1209). *Paleoceanogr. Paleoclimatol.* **33**, 626–642 (2018).

54. R. D. Norris, P. A. Wilson, P. Blum, Expedition 342 Scientists, in *Proceedings of the Integrated Ocean Drilling Program, Volume 342*, R. D. Norris, P .A. Wilson, P. Blum; Expedition 342 Scientists, Eds. (Integrated Ocean Drilling Program, 2014); http://publications.iodp.org/proceedings/342/342toc.htm.

55. J. A. Burnett, Upper Cretaceous, in *Calcareous Nannofossil Biostratigraphy,* P. R. Bown, Ed. (Kluwer Academic Publishers, 1998), pp. 132–165.

56. G. Bernaola, S. Monechi, Calcareous nannofossil extinction and survivorship across the Cretaceous−Paleogene boundary at Walvis Ridge (ODP Hole 1262C, South Atlantic Ocean). *Palaeogeogr. Palaeoclimatol. Palaeoecol.* **255**, 132–156 (2007).

57. N. Thibault, S. Gardin, The calcareous nannofossil response to the end-Cretaceous warm event in the Tropical Pacific. *Palaeogeogr. Palaeoclimatol. Palaeoecol.* **291**, 239–252 (2010).

58. S. J. Gibbs, A. J. Poulton, P. R. Bown, C. J. Daniels, J. Hopkins, J. R. Young, H. L. Jones, G. J. Thiemann, S. A. O'Dea, C. Newsam, Species-specific growth response of coccolithophores to Palaeocene–Eocene environmental change. *Nat. Geosci.* **6**, 218–222 (2013).

59. S. Våge, M. Castellani, J. Giske, T. F. Thingstad, Successful strategies in size structured mixotrophic food webs. *Aquat. Ecol.* **47**, 329–347 (2013).

60. B. A. Ward, M. J. Follows, Marine mixotrophy increases trophic transfer efficiency, mean organism size, and vertical carbon flux. *Proc. Natl. Acad. Sci. U.S.A.* **113**, 2958–2963 (2016).

61. C. T. Reinhard, N. J. Planavsky, B. A. Ward, G. D. Love, G. Le Hir, A. Ridgwell, The impact of marine nutrient abundance on early eukaryotic ecosystems. *Geobiology* **18**, 139–151 (2020).

62. P. J. Hansen, P. K. Bjørnsen, B. W. Hansen, Zooplankton grazing and growth: Scaling with the 2–2,000-µm body size range. *Limnol. Oceanogr.* **42**, 687–704 (1997).

63. B. W. Hansen, P. K. Bjornsen, P. J. Hansen, The size ratio between planktonic predators and their prey. *Limnol. Oceanogr.* **39**, 395–403 (1994).

64. K. F. Edwards, M. K. Thomas, C. A. Klausmeier, E. Litchman, Allometric scaling and taxonomic variation in nutrient utilization traits and maximum growth rate of phytoplankton. *Limnol. Oceanogr.* **57**, 554–566 (2012).

65. D. K. Stoecker, Acquired phototrophy in aquatic protists. *Aquat. Microb. Ecol.* **57**, 279–310 (2009).

66. J. D. van der Laan, P. Hogeweg, Predator—Prey coevolution: Interactions across different timescales. *Proc. R. Soc. Lond. B.* **259**, 35–42 (1995).

67. B. Sauterey, B. Ward, J. Rault, C. Bowler, D. Claessen, The implications of eco-evolutionary processes for the emergence of marine plankton community biogeography. *Am. Nat.* **190**, 116–130 (2017).

68. K. Hagino, J. R. Young, P. R. Bown, J. Godrijan, D. K. Kulhanek, K. Kogame, T. Horiguchi, Re-discovery of a "living fossil" coccolithophore from the coastal waters of Japan and Croatia. *Mar. Micropal.* **116**, 28–37 (2015).

69. N. A. Kamennaya, G. Kennaway, B. M. Fuchs, M. V. Zubkov, "Pomacytosis"—Semi-extracellular phagocytosis of cyanobacteria by the smallest marine algae. *PLOS Biol.* **16**, e2003502 (2018).

70. K. Hagino, R. Onuma, M. Kawachi, T. Horiguchi, Discovery of an endosymbiotic nitrogen-fixing cyanobacterium UCYN-A in *Braarudosphaera bigelowii* (Prymnesiophyceae). *PLOS ONE* **8**, e81749 (2013).

71. C. Linnert, J. Mutterlose, Boreal Early Turonian calcareous nannofossils from nearshore settings – Implications for paleoecology. *PALAIOS* **30**, 728–742 (2015).

72. H. Andruleit, S. Stäger, U. Rogalla, P. Čepek, Living coccolithophores in the northern Arabian Sea: Ecological tolerances and environmental control. *Mar. Micropal.* **49**, 157–181 (2003).

73. H. Mai, K. S. Perch-Nielsen, H. Willems, T. Romein, Fossil coccospheres from the K/T boundary section from Geulhemmerberg, The Netherlands. *Micropaleontology* **43**, 281–302 (1997).

74. J. Monod, La technique de culture continue, théorie et applications. *Ann. Inst. Pasteur* **79**, 390–410 (1950).

75. C. S. Holling, Some characteristics of simple types of predation and parasitism. *Can. Entomol.* **91**, 385–398 (1959).

76. W. C. Gentleman, A. B. Neuheimer, Functional responses and ecosystem dynamics: How clearance rates explain the influence of satiation, food-limitation and acclimation. *J. Plankton Res.* **30**, 1215–1231 (2008).

77. E. Marañón, P. Cermeño, D. C. López-Sandoval, T. Rodríguez-Ramos, C. Sobrino, M. Huete-Ortega, J. M. Blanco, J. Rodríguez, Unimodal size scaling of phytoplankton growth and the size dependence of nutrient uptake and use. *Ecol. Lett.* **16**, 371–379 (2013).

78. K. W. Wirtz, Non-uniform scaling in phytoplankton growth rate due to intracellular light and CO_2 decline. *J. Plankton Res.* **33**, 1325–1341 (2011).

79. D. E. Burmaster, The continuous culture of phytoplankton: Mathematical equivalence among three steady-state models. *Am. Nat.* **113**, 123–134 (1979).

80. B. A. Ward, E. Marañón, B. Sauterey, J. Rault, D. Claessen, The size dependence of phytoplankton growth rates: A trade-off between nutrient uptake and metabolism. *Am. Nat.* **189**, 170–177 (2017).

81. K. H. Andersen, J. E. Beyer, Asymptotic size determines species abundance in the marine size spectrum. *Am. Nat.* **168**, 54–61 (2006).

82. A. Beckmann, C.-E. Schaum, I. Hense, Phytoplankton adaptation in ecosystem models. *J. Theor. Biol.* **468**, 60–71 (2019).

83. N. Hamilton, Mesozoic magnetostratigraphy of Maud Rise, Antarctica, in *Proceedings of the Ocean Drilling Program, Scientific Results*, P. F. Barker, J. P. Kennett, Eds. (Ocean Drilling Program, 1990), vol. 113, pp. 255–260.

84. F. M. Gradstein, J. G. Ogg, M. D. Schmitz, G. M. Ogg, *The Geologic Time Scale 2012* (Elsevier, 2012).

85. R. D. Norris, D. Kroon, A. Klaus, Expedition 171B Scientists, in *Proceedings of the Ocean Drilling Programs Initial Reports, 171B*, R. D. Norris, D. Kroon, A. Klaus, Expedition 171B Scientists, Eds. (Integrated Ocean Drilling Program, 1998).